

Measurement of the binding force between RAS protein and a pathologic BRAF mutant using optical tweezers

Cheng Wen (闻 丞)^{1,2*} and Anpei Ye (叶安培)¹

¹Key Laboratory for the Physics & Chemistry of Nano-devices, School of Electronic Engineering and Computer Science, Peking University, Beijing 100871, China

²School of Life Sciences, Peking University, Beijing 100871, China

*Corresponding author: ailaowolf@163.com

Received April 22, 2013; accepted July 12, 2013; posted online August 28, 2013

Activating mutants in rat sarcoma (RAS) and B-rapid accelerated fibrosarcoma (BRAF) are found in at least a third of cases of human tumors and melanoma; hence, numerous therapeutic treatments target this pathway. In this letter, we study the adhesion force of RAS-coated beads with BRAF-coated beads, BRAF (A246P) mutant-coated beads, and GST-coated beads using optical tweezers. One full and two fractional RAS-BRAF specific binding modes are identified using the rupture force distribution. The $k_{\text{off}}(0)$ of the full binding mode in RAS-BRAF is $3.71 \times 10^{-4}/\text{s}$ and $1.16 \times 10^{-4}\text{s}^{-1}$ in RAS-BRAF (A246P), whereas the x_b is around 3×10^{-10} m in both groups.

OCIS codes: 170.0170, 170.1420.

doi: 10.3788/COL201311.091702.

Epidermal growth factor (EGF) receptors (EGFRs) transmit extracellular signals into the cell, leading to various cellular responses, e.g., cell proliferation, differentiation, and apoptosis^[1]. The downstream RAS-RAF-MEK (mitogen-activated protein kinase kinase)-ERK (Extracellular signal-regulated kinase) pathway is an attractive target for therapeutic intervention in oncology^[2]. Rat sarcoma (RAS) is a small guanosine triphosphatase (GTPase)^[3]. The active guanosine triphosphate (GTP)-bound RAS (RAS-GTP) interacts with effector molecules, e.g., B-rapid accelerated fibrosarcoma (BRAF), that trigger the activation of kinases MEK and ERK^[4-6]. Previous studies have revealed that RAF binds to RAS-GTP via two domains, the RAS-binding domain (RBD)^[7,8] and the cysteine-rich domain (CRD)^[9]. Both domains bind to RAS-GTP with high affinity, but the RBD-RAS bond is stronger^[10]. BRAF (A246P) is a rapid accelerated fibrosarcoma (RAF) mutant identified among patients with cardio-facio-cutaneous syndrome that differs from wild-type BRAF at its 246th amino acid residue in the CRD: the Ala (A) at the 246th position in wild-type BRAF is replaced with Pro (P) in BRAF (A246P)^[11]. Although the K_d values of the RAS-BRAF (full sequence) complex has been measured^[12], the unstressed off rate $k_{\text{off}}(0)$ and the reaction compliance x_b of the RAS-BRAF(A246P) bond remains unreported.

Optical tweezers are arguably the most versatile single-molecule manipulation technique; which can exert forces in excess of 100 pN on particles ranging in size from 10^{-9} to 10^{-6} m^[13]. It can be used to impose a specific interaction between the trapped object and a fixed partner, as well as measuring the force resulting from the interaction^[14]. Optical tweezers have recently been used to study the stretching-unstretching force of macromolecules (usually several piconewtons, e.g. Ref. [15]), the binding force between peptides and living cells (usually several tens of piconewtons, e.g. Ref. [16]), and the binding force between proteins (sometimes exceeding 100

pN, e.g. Refs. [17-19]). However, techniques for measuring interactions between macromolecules using optical tweezers are still scarce. This letter aims to measure the force spectra of the adhesion force of RAS-GTP on trapped beads with BRAF (CRD+RBD) and its mutant on fixed beads using optical tweezers. The single bond property of the RAS-BRAF complex and the effects of A246P mutation are then derived from the rupture force spectra.

The measurements were performed with custom-built optical tweezers based on a modified inverted microscope (Axiovert 200, Zeiss, Germany) using a Nd:YAG laser (Continuum, USA) with a wavelength of 1064 nm and maximum output of 4 W as a trapping source (Fig. 1). The expanded beam was focused using a lens L3 (focal length: 180 mm) to the conjugate point of the microscope objective (100 \times oil immersion objective, N.A. 1.33, Zeiss, Germany), and then focused onto the focal plane.

A quadrant photodiode detector (QD, custom-built), a program-controlled three-dimensional (3D) piezoelectric transducer sample stage (3D-PZT, Nanonics Imaging, Israel) and a charge-coupled device (CCD, WV-PA410/G, Panasonic, Japan) were integrated for force-trace

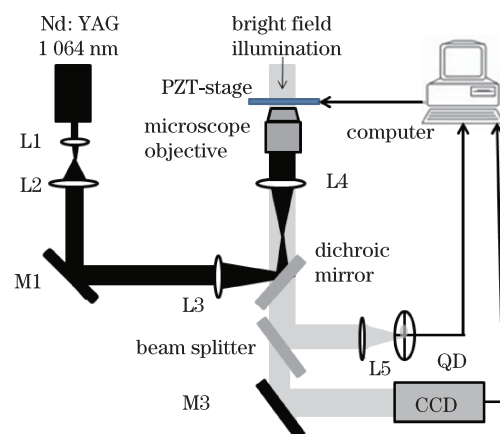


Fig. 1. Schematic of experimental setup.

recording and motion control. The samples were illuminated under bright-field microscopy and monitored using a CCD. The trapped bead was imaged on the QD panel to determine the displacement. The data acquisition of QD and the motion of the 3D-PZT sample stage were controlled by a computer with a DAQ card (NI-6229, National Instruments, USA) and a custom-developed LabView program. A MATLAB program was developed to convert the QD signal into a displacement profile, allowing the measurement of the force. The stiffness of optical tweezers k was calibrated with an acousto-optic deflector and a field programmable gateway following steps described in detail in a previous study^[20]. A stiffness of 0.4 pN/nm was achieved with an accuracy for positional measurement of around 1 nm.

The molecules of interest (GST-handled RAS, BRAF (CRD+RBD), and BRAF (A246P) (CRD+RBD) from Zhu's Lab, Medicine School of Virginia University, GST: glutathione S-transferase) were conjugated to the surface of functionalized micro-bead (carboxylated polystyrene, PS-COOH, 5 μm in diameter, Bangs, USA) respectively, via the following protocol. Firstly, 100 μL of 5% beads (w/v, suspended in deionized water) were washed in morpholino ethanesulfonic acid (MES) buffer. Then, the pellet was resuspended in 1 mL of activation buffer (12.5-mg *N*-hydroxysuccinimide (NHS), 7.8- μmol 1-(3-dimethylaminopropyl)-3-ethylcarbodiimide hydrochloride (EDC) and 20- μmol MES) and incubated at room temperature for 1 h. The beads were then washed in deionized water to remove excessive NHS and EDC. Finally, the beads were incubated with molecules of interest in Tris (hydroxymethyl) aminomethane and hydrochloride (Tris-HCl) buffer (pH=7.4) at 37 $^\circ\text{C}$ for 4 h and then washed in deionized water. The unreacted sites on the beads were blocked with bovine serum albumin (BSA, M&C Technology, Beijing, China). RAS-coated and GST-coated beads were employed in control experiments.

All the experiments were implemented in a sample cell mounted on the PZT sample stage. The cell chamber consisted of a modified Petri dish with a cover slip as bottom and another strip of cover slip vertically attached onto the bottom, which was immersed in 0.1% polylysine solution (M&C Technology, Beijing, China) in advance.

The following experimental procedures were repeated at least 2000 times to determine the rupture force distribution of RAS and BRAF using RAS-GTP/BRAF (CRD+RBD), RAS-GTP/BRAF (A246P) (CRD+RBD), RAS/BRAF (CRD+RBD) and GST/BRAF (CRD+RBD) beads. Firstly, the BRAF beads with Tris-HCl buffer (pH=7.4) were added into the chamber. They were trapped with optical tweezers, and manipulated onto the vertical surface of the polylysine-treated cover glass (Fig. 2). Secondly, the buffer solution and excess floating BRAF-beads were removed. RAS beads (or GST beads in control experiments) were added into 20 μL of 10-nM GTP solution (Sigma Aldrich, USA) in succession (or no GTP in the control experiments). Subsequently, driven by the PZT stage, a trapped bead was brought in contact with the fixed BRAF bead. After 1 s of contact, the separation was controlled by the Labview program, which provided the 3D-PZT a linear growth voltage signal, resulting in

horizontal movement at 5 $\mu\text{m}/\text{s}$. This movement leads to a loading rate of 2 nN/s on the trapped bead. If the "binding-unbinding" occurred between the two beads, a typical force-distance curve (Fig. 2(c)) was obtained, which can then be used to determine the rupture force.

The ratio of contact cases (adhesion rate), wherein the trapped bead attached to the fixed bead via either specific or nonspecific interaction, for the RAS-GTP/BRAF, RAS-GTP/BRAF (A246P), RAS/BRAF and GST/BRAF groups is shown in Fig. 3 (insert). The adhesion rates were significantly reduced in the RAS/BRAF and GST/BRAF groups. These experiments demonstrate that the contact cases in the former two groups could be mostly attributed to the interaction of RAS-GTP with BRAF or BRAF (A246P). Thus, the force measurements in these groups can reveal the feature of specific bond between RAS-GTP and BRAF as well as its mutant. The specificity of these interactions was verified.

The rupture force histogram of the aforementioned interactions at a loading rate 2 nN/s is shown in Fig. 3 (for the similarity in results of two control groups, the GST/BRAF group data is not shown). The rupture force in the nonspecific interaction (RAS/BRAF, Fig. 3) was weaker than the specific RAS-GTP-BRAF binding. On the other hand, the force in RAS-GTP-BRAF interaction (Fig. 3) was weaker than the RAS-GTP-BRAF (A246P) (Fig. 3) interaction. The nonspecific force was

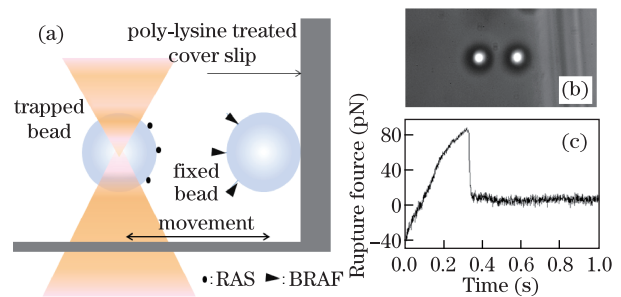


Fig. 2. (a) Schematic drawing for measuring the rupture force between trapped RAS beads and fixed BRAF beads using optical tweezers. (b) Micrograph of the measurement. (c) A typical rupture force trace acquired using QD for measurement.

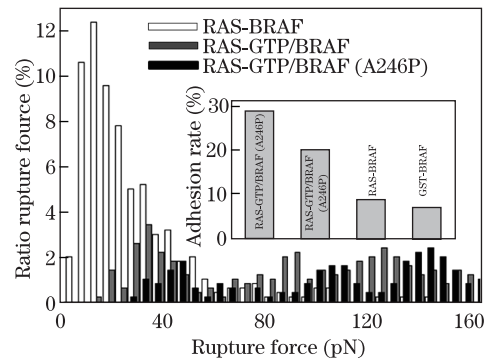


Fig. 3. Histogram of the rupture force distribution of RAS-BRAF, RAS-GTP-BRAF, and RAS-GTP-BRAF (A246P) interactions after a contact time of 1 s at a loading rate of 2 nN/s. Inset: Adhesion rates for RAS-GTP-BRAF, RAS-GTP-BRAF (A246P), RAS-BRAF, and GST-BRAF interactions.

usually less than 25 pN, whereas the specific force distribution was the superimposition of several pockets, exceeding 100 pN.

As determined in previous studies, the RBD or CRD in BRAF molecules bind independently to RAS^[10]. Considering the stochastic process of single molecular force measurement, four types of specific molecular associations occur upon contact of the RAS bead with the BRAF bead: 1. RAS and BRAF (RBD); 2. RAS and BRAF (CRD); 3. RAS and BRAF (RBD+CRD); 4. Stochastic combination of molecular associations described in cases 1–3. Since the affinity of multiple RAS–BRAF bonds (RAS–BRAF, $k_d < 6 \times 10^{-4} / \text{s}$ ^[12] vs. RGD peptide–cell surface, $k_d = 1.5 \times 10^{-2} / \text{s}$ ^[16]) may exceed the maximum force that optical tweezers can exert, and RAS beads rarely adhere onto BRAF beads (<5%), the rate of multiple bonds in our measurement is negligible. Hence, the binding modes of cases 1–3 dominate the specific interactions in the measurement, resulting in the first three prominent pockets in the force histogram of RAS–GTP–BRAF and RAS–GTP–BRAF (A246P) interactions.

The rupture force in each pocket in Fig. 3 was subjected to a Lilliefors' test. The result reveals that the bins in each pocket were approximately normally distributed ($p < 0.05$) and could be fitted to the curve

$$f[x, \mu_{i=1,2,3}, \sigma, k_{i=1,2,3}] = \sum_{i=1}^3 k_i \cdot e^{-\frac{(x-\mu_i)^2}{2\sigma^2}}. \quad (1)$$

The fitted means of each pocket in the RAS–GTP–BRAF and RAS–GTP–BRAF (A246P) histogram are shown in Table 1. In both cases, the sum of the mean of the first pocket (μ_1) and that of the second pocket (μ_2) is almost equal to the mean of the third (μ_3). This supports the model wherein the first pocket in the histogram corresponds to the weaker RAS–BRAF (CRD) bond, the second to the stronger RAS–BRAF (RBD) bond, whereas the third corresponds to the binding between RAS and BRAF (CRD+RBD).

The fitting of rupture force histogram is based on Eq. (1), with $k_1=0.86$, $k_2=0.56$, $k_3=0.75$ in the RAS/BRAF group, $k_1=0.31$, $k_2=0.33$, $k_3=0.43$ in the RAS/BRAF (A246P) group, and $\sigma=8.5$ pN in both cases.

Alternatively, following the one-step master equation

$$\frac{dp_i}{dt} = r_{i+1}p_i - r_i p_i, \quad (2)$$

where $p_i(t)$ is the possibility to find i closed bonds. The equation states that i decreases through the rupture of a closed bond with the rate $r_i = ik_{\text{off}} = ik_{\text{off}}(0)\exp(mt/iF_0)$ (inferred from Bell's model^[21]), where $k_{\text{off}}(0)$ is the unstressed off-rate, m is the loading rate, and $F_0 = k_{\text{off}}(0) \cdot x_b$ is the intrinsic force of the bond. The model derived from Eq. (2) provides the probability density for the rupture

Table 1. Mean Rupture Force for Pockets 1–3 in the RAS–GTP–BRAF and RAS–GTP–BRAF (A246P) Interaction Histograms

BRAF Species	μ_1 (pN)	μ_2 (pN)	μ_3 (pN)	$\mu_1 + \mu_2$ (pN)	P	R^2
BRAF (WT)	36	88	128	124	<0.01	0.75
BRAF (A246P)	48	110	150	158	<0.01	0.78

force f of initial number of closed bonds N_t ^[22]:

$$D(f) = \sum_{N_t=1}^{N_{tm}} p_\alpha(N_t) D_{N_t}(f) = \sum_{N_t=1}^{N_{tm}} P_\alpha(N_t) \frac{k_{\text{off}}(0)}{m} \cdot \exp\left(\frac{fx_b}{k_B T}\right) \exp\left\{\frac{k_{\text{off}}(0)}{m} \frac{k_B T}{x_b} \left[1 - \exp\left(\frac{fx_b}{k_B T}\right)\right]\right\}, \quad (3)$$

where k_B is the Boltzmann constant, T is the absolute temperature, x_b is the reactive compliance, $k_{\text{off}}(0)$ is the unstressed off rate. N_{tm} is the maximal number of initial bonds. $p_\alpha(N_t)$ is the coefficient determined by

$$p_\alpha(N_t) = \alpha_{N_t} / (\alpha_1 + \alpha_2 + \dots + \alpha_{N_{tm}}) \quad (4)$$

In this case, as previously discussed, only the RAS–BRAF (CRD), RAS–BRAF (RBD), and RAS–BRAF (CRD+RBD) binding modes dominate the experimental procedures. Equation (3) can be simplified as

$$D(f) = p_{\alpha\text{CRD}}(1)D_{1\text{CRD}}(f) + p_{\alpha\text{RBD}}(1)D_{1\text{RBD}}(f) + p_{\alpha\text{CRD+RBD}}(1)D_{1\text{CRD+RBD}}(f) + \varepsilon(f), \quad (5)$$

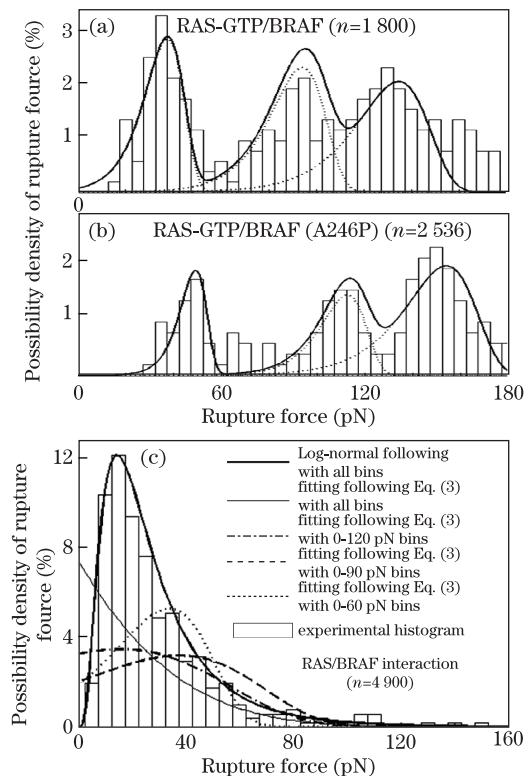


Fig. 4. (a) Rupture force histograms of the RAS–GTP–BRAF interactions at a loading rate of 2 nN/s, which include 500 binding–unbinding events from a total of 1800 attachment events. (b) Rupture force histograms of the RAS–GTP–BRAF (A246P) interactions at a loading rate of 2 nN/s, which include 500 binding–unbinding events from a total of 2536 attachment events. The dashed lines in (a) and (b) are fitting curves for each mode of specific binding pocket, whereas the solid lines are the simulation result according to the total data set via Eq. (3). (c) Rupture force histograms of the RAS–GTP–BRAF interactions at a loading rate of 2 nN/s, which include 410 binding–unbinding events from as total of 4900 attachment events. The solid dark lines in (a)–(c) are the possibility density functions simulated with the bins of histogram. The slender dashed lines in Fig. 4(c) show the results from different fitting strategies based on Eq. (3).

where $\varepsilon(f)$ is the fairly low possibility of multiple bonds.

Figures 4(a) and 4(b) show the simulated distribution curves using Eqs. (3) and (5). The least square fitting yielded an unstressed off-rate $k_{\text{off}}(0)=3.71\times 10^{-4}/\text{s}$ for the RAS-GTP-BRAF (CRD+RBD) association and $1.16\times 10^{-4}/\text{s}$ for RAS-GTP-BRAF (A246P) (CRD+RBD), whereas the x_b values were 3.2×10^{-10} m and 3.1×10^{-10} m, respectively. The results are in the same order of magnitude as previous results via the biochemical method for RAS and wild-type full-length BRAF ($k_{\text{d}}=5.76\times 10^{-4}/\text{s}$)^[12], and indicate that the BRAF (A246P) mutant binds to RAS-GTP more strongly than wild-type molecules.

Finally, as shown in Fig 4 (c), the experimental data for the RAS-BRAF interaction was well simulated with a Log Normal distribution $f(x, \mu, \sigma, k) = k \cdot \frac{1}{x\sigma} e^{-\frac{(\ln x - \mu)^2}{2\sigma^2}}$ ($k=0.40$, $\mu=3.14$, $\sigma=0.68$, $p<0.01$, $R^2=0.98$). However, Eq. (3) failed to simulate the force distribution of non-specific binding, which indicates that the nonspecific binding could not be described by the model derived from Eq. (3). On average, nonspecific interactions were weaker than specific ones, but exhibited a wider distribution and greater x_b values. It might serve as an important cofactor in the association of specific bond.

In conclusion, we demonstrate a case study on measuring the specific interactions between RAS and its downstream kinase BRAF using optical tweezers. The intrinsic physical parameters of the bond, $k_{\text{off}}(0)$ and x_b , are extracted from the experimental histogram of the rupture force. The result is comparable to the data derived using the biochemical method. Furthermore, threefold smaller $k_{\text{off}}(0)$ values are obtained for the RAS-BRAF (A246P) bond using the simulation of the experimental histogram. The lower $k_{\text{off}}(0)$ value for RAS-GTP-BRAF (A246P) bond indicates stronger binding between active RAS and the pathologic BRAF mutant, which needs to be inhibited with specific drugs that consider x_b in therapeutic treatments. The simple sample preparation method and force measurement strategy can be applied to a variety of studies on protein-protein interactions, especially for the quick identification of the biodynamic significance of pathologic protein mutants.

This work was supported by the Beijing Natural Science Foundation Project (No. 5102019). We thank Professor Zhu and Dr. Chae-Seok Lim of the University of Virginia for the RAS, BRAF (CRD+RBD), and BRAF (A246P) (CRD+RBD) protein samples used in this work, and Dr. Xu for the discussion on data processing.

References

1. C. Kiel and L. Serrano, *Sci. Sig.* **2**, ra38 (2009).
2. G. Hazivassiliou, K. Song, I. Yen, B. J. Brandhuber, D. J. Anderson, R. Alvarado, M. J. C. Ludlam, D. Stokoe, S. L. Gloor, G. Viger, T. Morales, I. Aliagas, B. Liu, S. Sideris, K. P. Hoefflich, B. S. Jaiswal, S. Seshagiri, H. Koeppe, M. Belvin, L. S. Friedman, and S. Malek, *Nature* **464**, 431 (2010).
3. P. A. Boriack-Sjodin, S. M. Margarit, D. Bar-Sagi, and J. Kuriyan, *Nature* **394**, 337 (1998).
4. W. Kolch, *Biochem. J.* **351**, 289 (2000).
5. D. R. Alessi, Y. Saito, D. G. Campbell, P. Cohen, G. Sithanandam, U. Rapp, A. Ashworth, C. J. Marshall, and S. Cowley, *EMBO J.* **13**, 1610 (1994).
6. L. Chang and M. Karin, *Nature* **410**, 37 (2001).
7. A. B. Vojtek, S. M. Hollenberg, and J. A. Cooper. *Cell* **74**, 205 (1993).
8. E. Chuang, D. Barnard, L. Hettich, X. Zhang, J. Avruch, and M. S. Marshall, *Mol. Cel. Biol.* **14**, 5318 (1994).
9. S. Ghosh, W. Xie, A. F. Quest, G. M. Mabrouk, J. C. Strum, and R. M. Bell, *J. Biol. Chem.* **269**, 10000 (1994).
10. T. R. Brtva, J. K. Drugan, S. Ghosh, R. S. Terrell, S. Campbell-Burk, R. M. Bell, and C. J. Der, *J. Biol. Chem.* **28**, 9809 (1995).
11. T. Niihori, Y. Aoki, Y. Narumi, G. Neri, H. Cavé, A. Verloes, N. Okamoto, R. C. M. Hennekam, G. Gillesen-Kaesbach, D. Wiczorek, M. I. Kavamura, K. Kurosawa, H. Ohashi, L. Wilson, D. Heron, D. Bonneau, G. Corona, T. Kaname, K. Naritomi, C. Baumann, N. Matsumoto, K. Kato, S. Kure, and Y. Matsubara, *Nature* **38**, 294 (2006).
12. A. Fischer, M. Hekman, J. Kuhlmann, I. Rubio, S. Wiese, and U. R. Rapp, *J. Biol. Chem.* **282**, 26503 (2007).
13. K. C. Neuman and A. Nagy, *Nat. Methods* **5**, 491 (2008).
14. J. R. Moffitt, Y. R. Chemla, S. B. Smith, and C. Bustamante, *Annu. Rev. Biochem.* **77**, 205 (2008).
15. C. Bustamante, Z. Bryant, and S. B. Smith, *Nature* **421**, 423 (2003).
16. M. Zhong, G. Xue, J. Zhou, Z. Wang, and Y. Li, *Chin. Opt. Lett.* **10**, 101701 (2012).
17. M. Salomo, U. F. Keyser, M. Struhalla, and F. Kremer, *Eur. Biophys J.* **37**, 927 (2008).
18. O. Björnham, J. Bugaytsova, T. Borén, and S. Schedin, *Biophys. Chem.* **143**, 102 (2009).
19. B. Shergill, L. Meloty-Kapella, A. A. Musse, G. Weinmaster, and E. Botvinick, *Dev. Cell.* **22**, 1313 (2012).
20. Q. Song, C. Wen, Y. Zhang, G. Wang, and A. Ye, *Chin. Opt. Lett.* **6**, 600 (2008).
21. G. I. Bell, *Science* **200**, 618 (1978).
22. T. Erdmann, S. Pierrat, P. Nassoy, and U. S. Schwarz, *Europhys. Lett.* **81**, 48001 (2008).